Mathematical modeling of serotonin compartmentation in normal human platelets

Geneviève Launay, J.L. Costa, M.D. Prada, J.M. Launay

INRIA

INSTITUT NATIONAL DE RECHERCHE EN INFORMATIQUE ET EN AUTOMATIQUE

Mathematical modeling of serotonin compartmentation in normal human platelets

Geneviève LAUNAY - Jonathan Lees COSTA
Mose Da PRADA - Jean-Marie LAUNAY

N° 1910
Mai 1993

PROGRAMME 5

Traitement du signal,
automatique et
productique

Mathematical modeling of serotonin compartmentation in normal human platelets

Modélisation du transport et du stockage de la sérotonine dans les plaquettes de sujets témoins

Geneviève Launay* Jonathan Lees Costa† Mose Da Prada‡
Jean-Marie Launay§

Abstract: The movement of radiolabelled 5-hydroxytryptamine (5-HT, serotonin) and its by-products between the extracellular medium, the thrombin-releasable (vesicular) compartment, and the non-thrombin-releasable compartment(s) has been investigated in normal human platelets.

Using the data obtained, identification of the kinetic constants for movement between the various compartments was possible. For carrying out the *a priori* identifiability analysis, a recent extension of similarity transformation approach to nonlinear compartmental models was used. Then numerical identification was performed by implementing and achieving efficient methods coming from optimal control theory.

Under our experimental conditions, the main results achieved are the following: 1) the vesicular compartment corresponds to the platelet storage 5-HT compartment, 2) instead of the pools I and II proposed previously only a single non-releseable thrombin-resistant pool could be detected and 3) the optimized model computed to suit the first set of experiments fits subsequent results obtained under similar experimental conditions.

Résumé : Les échanges de 5-hydroxytryptamine (5-HT, sérotonine) marquée et de ses dérivés entre le milieu extérieur, le compartiment (granulaire) libérable par la thrombine et le(s) compartiment(s) non sensible(s) à l'action de la thrombine ont été étudiés dans les plaquettes de sujets témoins.

A partir des données obtenues, une identification des coefficients d'échange entre les différents compartiments a été effectuée. Une extension récente de la méthode de changement de base dans l'espace d'état aux modèles compartimentaux non linéaires a été utilisée pour étudier l'identifiabilité structurelle. Puis une identification numérique a été faite par implémentation et mise en oeuvre de méthodes issues de la théorie du contrôle optimal.

Dans nos conditions expérimentales, les principaux résultats obtenus sont les suivants : 1) le compartiment granulaire correspond au stockage de la 5-HT plaquettaire, 2) au lieu des sites I et II proposés initialement, seul un compartiment non sensible à l'action de la thrombine a pu être détecté, 3) le modèle obtenu par optimisation à partir d'une première série de mesures conduit à un bon ajustement de résultats obtenus ultérieurement dans des conditions expérimentales similaires.

*INRIA, Domaine de Voluceau, BP 105, 78153 Rocquencourt - France

†Clinical Neuropharmacology Branch, NIMH, NIH Clinical Center, Bethesda, MD 20892 - present address Schwab Rehabilitation Center, Chicago, IL 60608 - USA

‡Pharmaceutical Research Department, F. Hoffmann-La Roche & Co. Ltd., CH-4002, Basel - Switzerland

§F.R.A. C. Bernard "Neurochimie des Communications Cellulaires", Hôpital St-Louis, 75010 Paris - France

Introduction

Blood platelets fulfill the prerequisites for being considered as a relatively simple and relevant model for pharmacological studies aiming to clarify basic mechanisms occurring at central serotoninergic neurons. Human platelets possess at least three "organelles" which are closely related in their functions to those of serotoninergic neurons :

(i) the cytoplasmic membrane with an active transport system for serotonin (5-hydroxytryptamine, 5-HT) and with binding sites for drugs and neurotransmitters,

(ii) subcellular vesicles (also called dense granules) which store 5-HT and other monoamines using a protontranslocating ATPase,

(iii) mitochondria with monoamine oxidase, the enzyme which catabolizes monoamines by oxidative deamination.

The use of human platelets to study drugs interfering with the active transport of monoamines, their storage sites, or their metabolism is facilitated by the fact that blood platelets are easily obtained by venipuncture. For this reason, platelets offer a useful model for clinical studies. To date, however, the utilization of platelets as a biological marker for well-established physiopathological states e.g. arteriosclerosis, hypertension and psychiatric disorders is still controversial (25). As a matter of fact, several methodological biases make difficult the interpretation of the experimental results. These pitfalls include diagnostic specificity , the normal physiological variability of age- and hormone-related changes, circadian and seasonal rhythms and unspecific drug effects. In addition, the knowledge about many biochemical mechanisms underlying platelet physiology is still fragmentary.

Based upon techniques for the abrupt inhibition of 5-HT uptake into platelets by formaldehyde fixation (5) and for the evaluation of 5-HT storage in vesicles by brief thrombin treatment (6), Costa et al. (8) postulated a model to describe the relationships between releasable and non-releasable pools of 5-HT in human platelets. The present study was designed to define in more detail the uptake pathways, compartmentation and possible inter-compartment movements of 5-HT in normal human platelets. The nonlinear differential equations obtained from the compartmental model proposed by Costa et al. (8) depend on unknown kinetic constants. Therefore we tackled an identifiability problem that was solved structurally first, using a recent extension of the similarity transformation approach to nonlinear compartmental models (29). Then numerical identification was performed by implementing and achieving efficient methods coming from optimal control theory (16).

1 Materials, theory and methods

1.1 Experimental protocol

- Three sets of experiments, designated M_1, M_2, M_3 were performed.
  For each set of experiments, eight volunteers (with no known history of haematological disorders or drug ingestion for at least two weeks before donation) were selected. Whole blood was collected into the citrate-EDTA medium of Detwiler & Feinman (13). Platelet-rich plasma and washed platelets were prepared by serial centrifugation at 4° C (23).

- For all experiments, 10^7 washed platelets in different volumes of buffer were incubated at 37° C in a shaking water bath with 2×10^{-7} M of [1,2−^{3}H]5-HT binoxalate (23.7 Ci/mmole, N.E.N. - Boston, Massachusetts, U.S.A.) during various times (expressed in seconds) :

$$\begin{cases} (10, 20, 30, 40, 60, 180, 300, 600, 900, 1200, 1800) & \text{for } M_1, M_2 \\ (10, 20, 30, 40, 60, 120, 300, 600, 1800) & \text{for } M_3 \end{cases} \quad (1)$$

Final volumes were 200 μl for M_1, M_3 and 1100 μl for M_2, giving platelet concentrations of 5×10^7 platelets/ml for M_1 and M_3 and 9.1×10^6 platelets/ml for M_2.
In the case of M_2 we increased the initial amount of [^{3}H]5-HT per platelet in the external medium, while keeping a saturating 5-HT initial concentration of 2×10^{-7} M.

- For all experiments, the reaction was stopped by formaldehyde (5) and platelets were separated from the incubation medium (6).

- For M_1 and M_2, two measurements were performed :

1. the tritiated material present in the platelets was determined by liquid scintillation counting (8),
2. the previous protocol was followed after a brief thrombin treatment of the platelets as described in (5), (6). The percent release of vesicles induced by thrombin was determined by electron microscopy (7) (air-dried whole mounts) and was taken into account. Thus, the amount of non-releasable intra-platelet tritiated material was measured.

- For M_3, two additional measurements were performed :

3. the amount of extra-platelet tritiated material was determined by liquid scintillation counting,
4. the amount of extra-platelet [^{3}H]5-HT was measured by radiochromatography (15).

- Each amount was determined in quadruplicate.

1.2 Mathematical model

The following diagram (see Fig. 1) was obtained from the compartmental system proposed by Costa et al. (8).

In the model described in Fig. 1

- All the exchanges were assumed to be linear except the uptake, where Michaelis terms were added according to previously-published information on the uptake of 5-HT by platelets (e.g. (28), (1)).

- x_0 is the amount of extra-platelet [^{3}H]5-HT,
e is the amount of extra-platelet tritiated material (i.e. tritiated material that came out from the platelets plus tritiated 5-HT that has not yet entered the platelets).
$x_i (1 \leq i \leq 3)$ is the amount of tritiated material (i.e. tritiated 5-HT plus tritiated 5-HT-derivatives) present in compartment i.

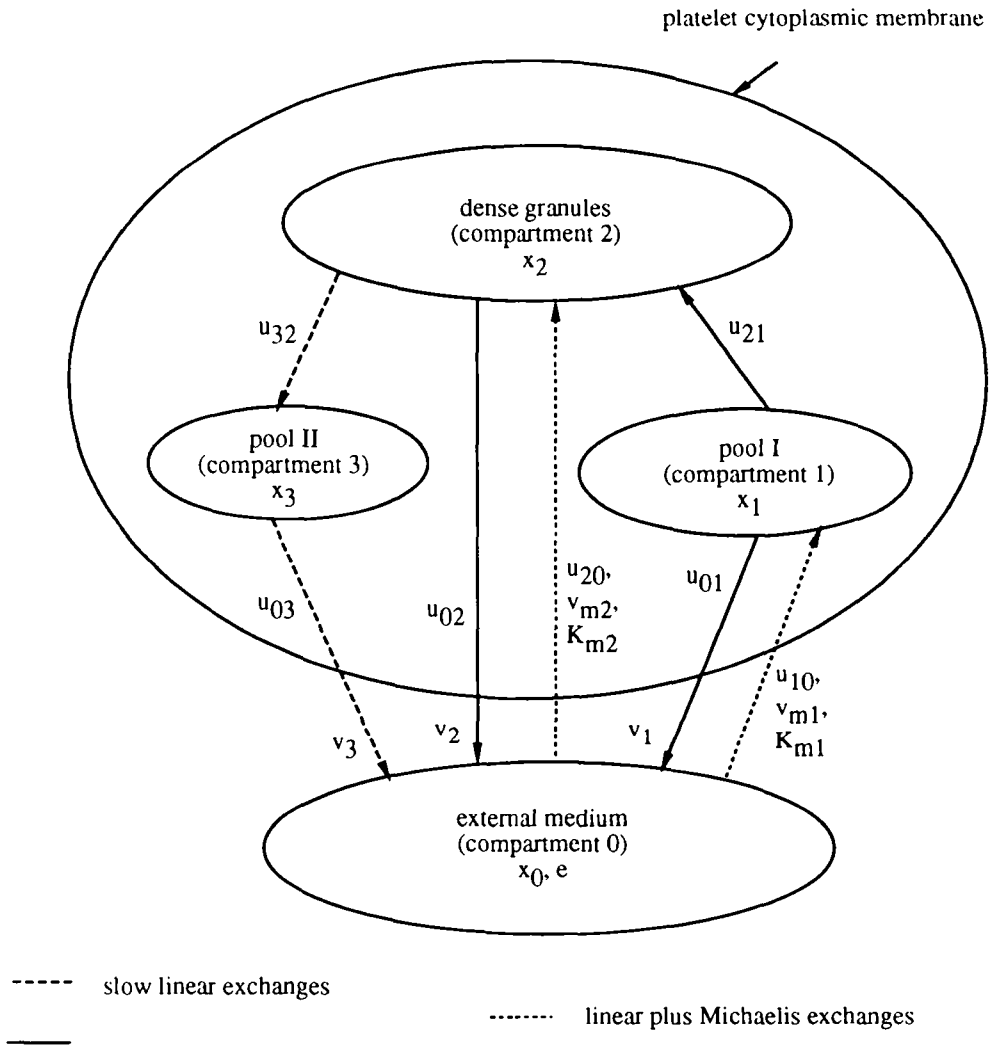

Figure 1: Proposed model for the uptake and storage of 5-HT in normal human platelets

- According to these notations, we know from the experimental protocol that denoting by $\hat{y}$ the observation, we have

$$\begin{cases} \hat{y} = (x_1 + x_2 + x_3 \ , \ x_1 + x_3) & \text{for } M_1 \text{ and } M_2 \\ \hat{y} = (x_1 + x_2 + x_3 \ , \ x_1 + x_3 \ , \ c \ , \ x_0) & \text{for } M_3 \end{cases} \tag{2}$$

the initial conditions (expressed in 10^{-19} mol/platelet) are

$$\begin{cases} x_0(0) = 40 \ , \ x_1(0) = x_2(0) = x_3(0) = 0 & \text{for } M_1 \\ x_0(0) = 220 \ , \ x_1(0) = x_2(0) = x_3(0) = 0 & \text{for } M_2 \\ x_0(0) = c(0) = 40 \ , \ x_1(0) = x_2(0) = x_3(0) = 0 & \text{for } M_3 \end{cases} \tag{3}$$

- $u_{i0}(1 \leq i \leq 2)$ is the rate coefficient for linear transfer of extra-platelet [^{3}H]-5-HT which comes in compartment i as tritiated material.
$v_{i0}^m, K_{i0}^m (1 \leq i \leq 2)$ are the constants for Michaelis transfer of extra-platelet [^{3}H]-5-HT which comes in compartment i as tritiated material.
$u_{ij}, (i,j) \in \{(2,1),(3,2),(0,1),(0,2),(0,3)\}$ is the rate coefficient for linear transfer of tritiated material from compartment j to compartment i,
$v_i (1 \leq i \leq 3)$ is the rate coefficient for linear transfer of tritiated material from compartment i which comes in the external medium as [^{3}H]5-HT .
Any of these coefficients is clearly nonnegative, and

$$\text{for all } i \in \{1,2,3\} \quad 0 \leq v_i \leq u_{0i} \tag{4}$$

These constraints (Eq. 4) are difficult to take into account in a procedure of numerical identification because the upper bounds u_{0i} of the unknowns v_i are also unknowns to be identified.

Then considering $\alpha_i (1 \leq i \leq 3)$ the ratio of tritiated 5-HT to tritiated material coming back to the external medium from compartment i, we get

$$v_i = \alpha_i u_{0i} \tag{5}$$

and Equation 4 becomes

$$\text{for all } i \in \{1,2,3\} \quad 0 \leq \alpha_i \leq 1 \tag{6}$$

- From these notations and assumptions, the model described in Fig. 1 yields the following state-equations

$$\begin{cases} \dfrac{dx_0}{dt} = -\left(u_{10} + \dfrac{v_{10}^m}{K_{10}^m + x_0} + u_{20} + \dfrac{v_{20}^m}{K_{20}^m + x_0}\right) x_0 + v_1 x_1 + v_2 x_2 + v_3 x_3 & (7) \\ \dfrac{dx_1}{dt} = \left(u_{10} + \dfrac{v_{10}^m}{K_{10}^m + x_0}\right) x_0 - (u_{21} + u_{01}) x_1 & (8) \\ \dfrac{dx_2}{dt} = \left(u_{20} + \dfrac{v_{20}^m}{K_{20}^m + x_0}\right) x_0 - (u_{32} + u_{02}) x_2 + u_{21} x_1 & (9) \\ \dfrac{dx_3}{dt} = u_{32} x_2 - u_{03} x_3 & (10) \end{cases}$$

and a fifth equation (for M_3) that gives e

$$\frac{de}{dt} = -\left(u_{10} + \frac{v_{10}^m}{K_{10}^m + x_0} + u_{20} + \frac{v_{20}^m}{K_{20}^m + x_0}\right) x_0 + u_{01}x_1 + u_{02}x_2 + u_{03}x_3 \qquad (11)$$

- It is well-known that the molecule of 5-HT is liable to degradation (32) and that a number of platelet-derived molecules bind 5-HT with a high degree of affinity and specificity (26), (20).

  So we considered first a simplified case where we assumed that there is no 5-HT in the tritiated material coming out from the platelets : this assumption is equivalent to setting

  $$v_1 = v_2 = v_3 = \alpha_1 = \alpha_2 = \alpha_3 = 0$$

  Then we considered the general case where the $\alpha_i (1 \leq i \leq 3)$ are unknowns to be identified, subject to the constraints of Equation 6.

- Notice that the unlabelled 5-HT present in the platelets prior to any experiment never appears in the measurements nor in the state-equations (Eq. 7-11). Indeed, the basic assumption of this study is the expectation that there is no unusual movement of unlabelled 5-HT during the tests.

1.3 Identification aspects

Classically (17) two distinct aspects of any identifiability problem are considered

- The structural identifiability analysis tests the global or local uniqueness of solutions for the parameters of a given model from noise-free data corresponding to a specified class of input-output experiments. These structural identifiability conditions (which deal with theoretical noise-free data) are minimal and necessary for achieving meaningful estimation of model parameters from real noisy data.

- The identifiability question in the presence of real, noisy data is often referred to as numerical identifiability ; it is the same (in the context of parameter estimation) as the problem of parameter estimation precision, given that the parameters are known to be structurally identifiable. Then a parameter u_0 is considered to be numerically unidentifiable if and only if the fractional standard deviation of the parameter estimate $\sqrt{\frac{v_0}{u_0}}$ exceeds 100 % (2) (v_0 is the standard deviation estimate of u_0).

2 Structural identification

2.1 Method

Definitions

Consider a model M of the form

$$\begin{cases} \frac{dx}{dt} = a(x,u) + v(t)b(x,u) \\ y = c(x,u) \\ X_0(u) \text{ is the initial value of } x \end{cases}$$

where :

t denotes the time variable,

$x(t,u) \in \mathbb{R}^{n_x}$ and $y(t,u) \in \mathbb{R}^{n_y}$ denote the state variables and the output respectively (so $X_0(u) = x(0,u) \in \mathbb{R}^{n_x}$),

v denotes a bounded and measurable function defined on the time interval $[0,t_1]$ (the single-input is considered for notational simplicity). Let $\mathcal{V}$ be the input class i.e. the set of possible values of the input map $v(.)$,

$u \in \mathbb{R}^{n_u}$ denotes the vector of parameters to be identified. Let $\Omega \subset \mathbb{R}^{n_u}$ be the set of possible parameter values.

Thus for any u selected in Ω, $X_0(u)$ is well defined so that the model $M(u)$ associates to any input map $v(.)$ in $\mathcal{V}$ an output map $y(.,u)$.

Then the parameter values u, $\tilde{u} \in \Omega$ are said to be indistinguishable for the input class $\mathcal{V}$ and for the initial conditions X_0 (denoted $[u \sim \tilde{u} \mid \mathcal{V}, X_0]$) iff :
[for all $v \in \mathcal{V}$, $y(.,u) = y(.,\tilde{u})$]

Model $M(u)$ is globally identifiable for $\mathcal{V}$ and X_0 at $u \in \Omega$ iff $[u \sim \tilde{u} \mid \mathcal{V}, X_0]$, $\tilde{u} \in \Omega$, implies $u = \tilde{u}$, and it is locally identifiable for $\mathcal{V}$ and X_0 at $u \in \Omega$ iff there exists a neighborhood Ω' of u in Ω such that $[u \sim \tilde{u} \mid \mathcal{V}, X_0]$, $\tilde{u} \in \Omega'$, implies $u = \tilde{u}$.

Model M is said to be globally (locally) structurally identifiable for $\mathcal{V}$ and X_0 iff it is globally (locally) identifiable for $\mathcal{V}$ and X_0 at almost any $u \in \Omega$, i.e. at all $u \in \Omega$ except the points of a subset of zero measure in Ω.

Similarity transformation approach

The similarity transformation approach of Walter and Lecourtier (30) applies to any linear time-invariant model L of the form

$$\begin{cases} \dfrac{dx}{dt} = A(u)x + B(u)v(t) \\ y(t) = C(u)x(t) \\ X_0(u) \text{ is the initial value of } x \end{cases}$$

which is supposed structurally controllable and observable. Then any controllable and observable model $L(\tilde{u})$ whose input-output map is equal to that of model $L(u)$ can be deduced from the model $L(u)$ by a state-space similarity transformation T (i.e. T is a linear map from $\mathbb{R}^{n_x}$ to $\mathbb{R}^{n_x}$ such that : (i) T is non singular, (ii) $TX_0(\tilde{u}) = X_0(u)$, and (iii) $TA(\tilde{u}) = A(u)T$, $TB(\tilde{u}) = B(u)$ and $C(\tilde{u}) = C(u)T$), so that the known system structure is preserved under feasible structure transformation. Thus constructing the family of feasible transformations, one finds all values $\tilde{u}$ such that $\tilde{u} \sim u$.

This similarity transformation approach was extended by Vajda et al. (29) in the following way

As for the linear case, it is necessary to assume that M satisfies some controllability and observability conditions so that M is minimal.

Result 1 General analysis for minimality can be avoided in the particular case where M is such that the functions a, b, c are analytic and there exists $u^* \in \Omega$ at which $M(u^*)$ becomes linear (i.e. of the form $L(u^*)$). Then controllability and observability of the linear model $M(u^*)$ is a sufficient condition for M to be minimal at $X_0(u) = 0$ for almost any $u \in \Omega$.

Then a sufficient and necessary condition for global identifiability of the nonlinear model M is the following

Result 2 Assume that the model $M(u)$ is minimal at $X_0(u)$ for almost any $u \in \Omega$. Consider the parameter values $u, \tilde{u} \in \Omega$, a neighborhood $\mathcal{X}$ of $X_0(\tilde{u})$ in $\mathbb{R}^{n_x}$, and any analytical mapping λ from $\mathcal{X} \subset \mathbb{R}^{n_x}$ to $\mathbb{R}^{n_x}$ such that for all $\tilde{x} \in \mathcal{X}$:

$$\begin{cases} Rank \dfrac{\partial \lambda}{\partial \tilde{x}}(\tilde{x}) = n_x & (12) \\ \lambda(X_0(\tilde{u})) = X_0(u) & (13) \\ \left.\begin{array}{ll} a(\lambda(\tilde{x}), u) = \dfrac{\partial \lambda}{\partial \tilde{x}}(\tilde{x}) a(\tilde{x}, \tilde{u}) & (14a) \\ b(\lambda(\tilde{x}), u) = \dfrac{\partial \lambda}{\partial \tilde{x}}(\tilde{x}) b(\tilde{x}, \tilde{u}) & (14b) \\ c(\lambda(\tilde{x}), u) = c(\tilde{x}, \tilde{u}) & (14c) \end{array}\right\} & (14) \end{cases}$$

Then there exists $t_1 > 0$ such that M is globally identifiable for the input class of all the bounded and measurable functions defined on $[0, t_1]$ and for the initial conditions $X_0(u)$ iff Equations 12-14 imply $\tilde{u} = u$.

So far, identifiability property is established under the assumption that the entire set of bounded and measurable functions defined on $[0, t_1]$ is available for input. However in most applications the input v is not arbitrary but is restricted to specific input functions (in our particular case of impulsive form). Nevertheless the previous sufficient and necessary condition enables identifiability to be studied in such experiments if the following restrictions hold :

$$\begin{cases} b(x, u) = b(u) \text{ i.e. the input is multiplied by a constant vector } b & (15) \\ a(0, u) = 0 \text{ i.e. with no input the system stays at rest} & (16) \\ \lambda(\tilde{x}) = T\tilde{x} \text{ where } T \text{ is an } n_x \times n_x \text{ constant nonsingular matrix} & (17) \end{cases}$$

Indeed the following result holds

Result 3 Let the model M satisfy the restrictive equations 15-17. If the model is globally identifiable at $u \in \Omega$ for the input class of all the bounded and measurable functions defined on $[0, t_1]$ and for $X_0 = 0$, then it is globally identifiable at $u \in \Omega$

- for the specified input v (where v is any function right continuous and non zero at the origin) and for $X_0 = 0$
- for a zero-input experiment ($v = 0$) with the initial condition $X_0(u) = b(u)$.

2.2 Carrying out

• **For M_1, M_2**
The model introduced in Section 1.2 for M_1, M_2 is globally structurally identifiable for the experimental input and initial conditions.

Proof : The considered model is of the form M with
$x = (x_0 \quad x_1 \quad x_2 \quad x_3)^T$ where ^{T} denotes the transpose matrix operation, and so $n_x = 4$.
$u = (u_{10} \quad u_{20} \quad u_{21} \quad u_{32} \quad u_{01} \quad u_{02} \quad u_{03} \quad v_{10}^m \quad K_{10}^m \quad v_{20}^m \quad K_{20}^m \quad v_1 \quad v_2 \quad v_3)^T$, and so $n_u = 14$.
Ω is the set of all the vectors of $\mathbb{R}^{14}$ with nonnegative entries.
$a(x,u)$ is the column vector of the right-hand sides of Equations 7-10.
$b(x,u) = b = (x_0(0) \quad x_1(0) \quad x_2(0) \quad x_3(0))^T$ constant vector with $x_0(0) \neq 0$ and
$x_1(0) = x_2(0) = x_3(0) = 0$ (Eq. 3).
$c(x,u) = (x_1 + x_2 + x_3 \quad x_1 + x_3)^T$ (Eq. 2),
and either a zero-input with the initial condition b, i.e.

$$\begin{cases} v = 0 \\ X_0(u) = b \end{cases} \tag{18}$$

or an impulse input at time 0 with a zero initial condition, i.e.

$$\begin{cases} v = \delta_0 \text{ Dirac measure at time 0} \\ X_0(u) = 0 \end{cases} \tag{19}$$

which are two approaches to describe the initial experimental protocol.

The first step is to check minimality conditions.
We use Result 1 (Section 2.1) since a, b, c are analytic and for any $u^* \in \Omega$ such that $v_{10}^m = v_{20}^m = 0$, the state-system becomes linear. Then selecting
$u^* = (1 \quad 2 \quad 3 \quad 4 \quad 5 \quad 6 \quad 7 \quad 0 \quad 1 \quad 0 \quad 1 \quad 0 \quad 0 \quad 0)$
we check that the associated linear state-system is controllable and observable by verifying that the controllability matrix $(B \quad AB \quad A^2B \quad A^3B)$ and the observability matrix $\begin{pmatrix} C \\ CA \\ CA^2 \\ CA^3 \end{pmatrix}$ are both of full rank 4. So we deduce from Result 1 (Section 2.1) that the considered model is minimal at $X_0(u) = 0$ for almost any $u \in \Omega$.

The next stage is to construct all the local transformations

$$\lambda(\tilde{x}) = (\lambda_0(\tilde{x}) \ \lambda_1(\tilde{x}) \ \lambda_2(\tilde{x}) \ \lambda_3(\tilde{x}))^T$$

that satisfy Equations 12-14 of Result 2 (Section 2.1).

Consider in this construction that Equations 19 give the input and initial conditions.

From the value of $c(x,u)$, Equation 14c reduces to

$$\begin{cases} \lambda_2(\tilde{x}) = \tilde{x}_2 \\ \lambda_1(\tilde{x}) + \lambda_3(\tilde{x}) = \tilde{x}_1 + \tilde{x}_3 \end{cases} \tag{20}$$

since $X_0(u)$ is the origin of $\mathbb{R}^4$ (Eq. 19), Equation 13 is

$$\lambda(0) = 0$$

From the value of $b(x,u) = b$, Equation 14b reduces to

$$\begin{cases} \dfrac{\partial \lambda_0}{\partial \tilde{x}_0}(\tilde{x}) = 1 \\ \dfrac{\partial \lambda_0}{\partial \tilde{x}_1}(\tilde{x}) = \dfrac{\partial \lambda_0}{\partial \tilde{x}_2}(\tilde{x}) = \dfrac{\partial \lambda_0}{\partial \tilde{x}_3}(\tilde{x}) = 0 \end{cases}$$

which, taking Equation 13 into account, implies

$$\lambda_0(\tilde{x}) = \tilde{x}_0 \tag{21}$$

Then plugging Equations 20-21 into Equation 14a gives

$$a(\lambda(\tilde{x}), u) = \begin{pmatrix} 1 & 0 & 0 & 0 \\ \frac{\partial \lambda_1}{\partial \tilde{x}_0}(\tilde{x}) & \frac{\partial \lambda_1}{\partial \tilde{x}_1}(\tilde{x}) & \frac{\partial \lambda_1}{\partial \tilde{x}_2}(\tilde{x}) & \frac{\partial \lambda_1}{\partial \tilde{x}_3}(\tilde{x}) \\ 0 & 0 & 1 & 0 \\ -\frac{\partial \lambda_1}{\partial \tilde{x}_0}(\tilde{x}) & 1 - \frac{\partial \lambda_1}{\partial \tilde{x}_1}(\tilde{x}) & -\frac{\partial \lambda_1}{\partial \tilde{x}_2}(\tilde{x}) & 1 - \frac{\partial \lambda_1}{\partial \tilde{x}_3}(\tilde{x}) \end{pmatrix} \times a(\tilde{x}, \tilde{u}) \tag{22}$$

to be satisfied for all $\tilde{x} \in \mathcal{X}$ a neighborhood of the origin in $\mathbb{R}^4$.

Equations 22 imply

$$\begin{cases} \text{[first equation]} \quad a_0(\lambda(\tilde{x}), u) = a_0(\tilde{x}, \tilde{u}) \\ \text{[third equation]} \quad a_2(\lambda(\tilde{x}), u) = a_2(\tilde{x}, \tilde{u}) \\ \text{[adding second and fourth equations]} \quad (a_1 + a_3)(\lambda(\tilde{x}), u) = (a_1 + a_3)(\tilde{x}, \tilde{u}) \end{cases} \tag{23}$$

for all $\tilde{x} \in \mathcal{X}$

Select $\tilde{x}_1 = \tilde{x}_2 = \tilde{x}_3 = 0$. Then Equations 20 yield $\lambda_2(\tilde{x}) = 0$ and $\lambda_3(\tilde{x}) = -\lambda_1(\tilde{x})$ so that, from the value of $a(x, u)$ and from Equation 21, Equations 23 reduce to

$$\begin{cases} -\left(u_{10} + \frac{v_{10}^m}{K_{10}^m + \tilde{x}_0} + u_{20} + \frac{v_{20}^m}{K_{20}^m + \tilde{x}_0}\right)\tilde{x}_0 + (v_1 - v_3)\lambda_1(\tilde{x}) = \\ -\left(\tilde{u}_{10} + \frac{\tilde{v}_{10}^m}{\tilde{K}_{10}^m + \tilde{x}_0} + \tilde{u}_{20} + \frac{\tilde{v}_{20}^m}{\tilde{K}_{20}^m + \tilde{x}_0}\right)\tilde{x}_0 \\ \left(u_{20} + \frac{v_{20}^m}{K_{20}^m + \tilde{x}_0}\right)\tilde{x}_0 + u_{21}\lambda_1(\tilde{x}) = \left(\tilde{u}_{20} + \frac{\tilde{v}_{20}^m}{\tilde{K}_{20}^m + \tilde{x}_0}\right)\tilde{x}_0 \\ \left(u_{10} + \frac{v_{10}^m}{K_{10}^m + \tilde{x}_0}\right)\tilde{x}_0 + (u_{03} - u_{21} - u_{01})\lambda_1(\tilde{x}) = \left(\tilde{u}_{10} + \frac{\tilde{v}_{10}^m}{\tilde{K}_{10}^m + \tilde{x}_0}\right)\tilde{x}_0 \end{cases} \tag{24}$$

which should be satisfied for all $\tilde{x}_0$ on some neighborhood of the origine in $\mathbb{R}$.
Then adding Equations 24 gives $(v_1 - v_3 + u_{21} + u_{03} - u_{21} - u_{01})\lambda_1(\tilde{x}) = 0$ and so we may consider $\lambda_1(\tilde{x}) = 0$ since the subset of Ω whose equation is $v_1 - v_3 + u_{21} + u_{03} - u_{21} - u_{01} = 0$ has zero measure.
So it turns out that Equations 24 imply for almost any $u \in \Omega$

$$u_{10} = \tilde{u}_{10}, \quad v_{10}^m = \tilde{v}_{10}^m, \quad K_{10}^m = \tilde{K}_{10}^m, \quad u_{20} = \tilde{u}_{20}, \quad v_{20}^m = \tilde{v}_{20}^m, \quad K_{20}^m = \tilde{K}_{20}^m \tag{25}$$

Select $\tilde{x}_0 = 0$. Then Equation 21 yields $\lambda_0(\tilde{x}) = 0$ and so, from the value of $a(x, u)$ and from Equations 20, Equations 23 reduce to

$$\begin{cases} v_1\lambda_1(\tilde{x}) + v_2\tilde{x}_2 + v_3(\tilde{x}_1 + \tilde{x}_3 - \lambda_1(\tilde{x})) = \tilde{v}_1\tilde{x}_1 + \tilde{v}_2\tilde{x}_2 + \tilde{v}_3\tilde{x}_3 \\ -(u_{32} + u_{02})\tilde{x}_2 + u_{21}\lambda_1(\tilde{x}) = -(\tilde{u}_{32} + \tilde{u}_{02}\tilde{x}_2) + \tilde{u}_{21}\tilde{x}_1 \\ -(u_{21} + u_{01})\lambda_1(\tilde{x}) + u_{32}\tilde{x}_2 - u_{03}(\tilde{x}_1 + \tilde{x}_3 - \lambda_1(\tilde{x})) = \\ -(\tilde{u}_{21} + \tilde{u}_{01})\tilde{x}_1 + \tilde{u}_{32}\tilde{x}_2 - \tilde{u}_{03}\tilde{x}_3 \end{cases} \tag{26}$$

which should be satisfied for all $(\tilde{x}_1, \tilde{x}_2, \tilde{x}_3)$ on some neighborhood of the origin in $\mathbb{R}^3$.

Then eliminating $\lambda_1(\tilde{x})$ between the first two and the last two equations of Equations 26 gives

$$\begin{cases} u_{21}|(\tilde{v}_1 - v_3)\tilde{x}_1 + (\tilde{v}_2 - v_2)\tilde{x}_2 + (\tilde{v}_3 - v_3)\tilde{x}_3| = (v_1 - v_3)|\tilde{u}_{21}\tilde{x}_1 + (u_{32} + u_{02} - \tilde{u}_{32} - \tilde{u}_{02})\tilde{x}_2| \\ (u_{03} - u_{21} - u_{01})|\tilde{u}_{21}\tilde{x}_1 + (u_{32} + u_{02} - \tilde{u}_{32} - \tilde{u}_{02})\tilde{x}_2| = \\ u_{21}|(u_{03} - \tilde{u}_{21} - \tilde{u}_{01})\tilde{x}_1 + (\tilde{u}_{32} - u_{32})\tilde{x}_2 + (u_{03} - \tilde{u}_{03})\tilde{x}_3| \end{cases}$$

which from the coefficients of $\tilde{x}_1, \tilde{x}_2$ gives

$$\begin{cases} u_{21}(\tilde{v}_1 - v_3) = \tilde{u}_{21}(v_1 - v_3) \\ (u_{03} - u_{21} - u_{01})\tilde{u}_{21} = (u_{03} - \tilde{u}_{21} - \tilde{u}_{01})u_{21} \\ u_{21}(\tilde{v}_2 - v_2) = (v_1 - v_3)(u_{32} + u_{02} - \tilde{u}_{32} - \tilde{u}_{02}) \\ (u_{03} - u_{21} - u_{01})(u_{32} + u_{02} - \tilde{u}_{32} - \tilde{u}_{02}) = u_{21}(\tilde{u}_{32} - u_{32}) \end{cases} \tag{27}$$

while the coefficients of $\tilde{x}_3$ give

$$\begin{cases} u_{21}(\tilde{v}_3 - v_3) = 0 \\ u_{21}(u_{03} - \tilde{u}_{03}) = 0 \end{cases} \text{ i.e. for almost any } u \in \Omega \begin{cases} v_3 = \tilde{v}_3 \\ u_{03} = \tilde{u}_{03} \end{cases} \tag{28}$$

For any $\tilde{x} \in \mathcal{X}$ neighborhood of the origin in $\mathbb{R}^4$, taking into account the value of $a(x,u)$ and Equations 20, 21, 25 and 28, Equations 23 reduce to

$$\begin{cases} v_1\lambda_1(\tilde{x}) + v_2\tilde{x}_2 + v_3(\tilde{x}_1 - \lambda_1(\tilde{x})) = \tilde{v}_1\tilde{x}_1 + \tilde{v}_2\tilde{x}_2 \\ -(u_{32} + u_{02})\tilde{x}_2 + u_{21}\lambda_1(\tilde{x}) = -(\tilde{u}_{32} + \tilde{u}_{02})\tilde{x}_2 + \tilde{u}_{21}\tilde{x}_1 \\ -(u_{21} + u_{01})\lambda_1(\tilde{x}) + u_{32}\tilde{x}_2 - u_{03}(\tilde{x}_1 - \lambda_1(\tilde{x})) = -(\tilde{u}_{21} + \tilde{u}_{01})\tilde{x}_1 + \tilde{u}_{32}\tilde{x}_2 \end{cases} \tag{29}$$

So the second of Equations 29 yields for almost any $u \in \Omega$

$$\lambda_1(\tilde{x}) = \frac{1}{u_{21}}[\tilde{u}_{21}\tilde{x}_1 + (u_{32} + u_{02} - \tilde{u}_{32} - \tilde{u}_{02})\tilde{x}_2]$$

from which, taking into account Equations 20, 21, 25 and 28, the second of Equations 22 reduces to

$$\begin{aligned} &\left(u_{10} + \frac{v_{10}^m}{K_{10}^m + \tilde{x}_0}\right)\tilde{x}_0 - \left(\frac{u_{21} + u_{01}}{u_{21}}\right)(\tilde{u}_{21}\tilde{x}_1 + (u_{32} + u_{02} - \tilde{u}_{32} - \tilde{u}_{02})\tilde{x}_2) = \\ &\frac{\tilde{u}_{21}}{u_{21}}\left[\left(u_{10} + \frac{v_{10}^m}{K_{10}^m + \tilde{x}_0}\right)\tilde{x}_0 - (\tilde{u}_{21} + \tilde{u}_{01})\tilde{x}_1\right] + \\ &\left(\frac{u_{32} + u_{02} - \tilde{u}_{32} - \tilde{u}_{02}}{u_{21}}\right)\left[\left(u_{20} + \frac{v_{20}^m}{K_{20}^m + \tilde{x}_0}\right)\tilde{x}_0 - (\tilde{u}_{32} + \tilde{u}_{02})\tilde{x}_2 + \tilde{u}_{21}\tilde{x}_1\right] \end{aligned} \tag{30}$$

which should be satisfied for all $(\tilde{x}_0, \tilde{x}_1, \tilde{x}_2)$ on some neighborhood of the origin in $\mathbb{R}^3$, and so which gives from the terms involving $\tilde{x}_0$

$$\begin{cases} u_{32} + u_{02} - \tilde{u}_{32} - \tilde{u}_{02} = \dfrac{u_{10}}{u_{20}}(u_{21} - \tilde{u}_{21}) \\ (u_{21} - \tilde{u}_{21})\left(v_{10}^m - \dfrac{u_{10}}{u_{20}}v_{20}^m\right) = 0 \\ (u_{21} - \tilde{u}_{21})\left(v_{10}^m K_{20}^m - \dfrac{u_{10}}{u_{20}}v_{20}^m K_{10}^m\right) = 0 \end{cases}$$

i.e. for almost any $u \in \Omega$

$$\begin{cases} u_{21} = \tilde{u}_{21} \\ u_{32} + u_{02} = \tilde{u}_{32} + \tilde{u}_{02} \end{cases} \tag{31}$$

Taking Equations 31 into account, coefficients of $\tilde{x}_1$ in Equation 30 give

$$u_{01} = \tilde{u}_{01} \tag{32}$$

Then plugging Equations 31-32 into Equations 27 gives

$$v_1 = \tilde{v}_1,\ v_2 = \tilde{v}_2,\ u_{32} = \tilde{u}_{32} \tag{33}$$

So from Equations 25, 28 and 31-33 it turns out that $u = \tilde{u}$. Thus from Result 2 (Section 2.1), the considered model is globally structurally identifiable for the input class of all the bounded and measurable functions defined on $[0, t_1]$ and for the considered initial conditions $X_0(u) = 0$ (Eq. 19).

Finally from Result 3, the considered model is globally structurally identifiable for a zero-input experiment ($v = 0$) with the initial conditions $X_0(u) = b(u) = b$, which from Equations 18 corresponds to the experimental input and initial conditions.

• **For M_3**
The model introduced in Section 1.2 for M_3 is globally structurally identifiable for the experimental input and initial conditions.
Proof : Equation 11 provides no more parameters than Equations 7-10. Moreover Equations 19 describe the initial experimental protocol as for M_1, M_2, and the output is $c(x,u) = (x_1+x_2+x_3 \quad x_1+x_3 \quad e \quad x_0)^T$ (Eq. 2) whose first two components are the same as in M_1, M_2. So we deduce the result for M_3 from the previous result for M_1, M_2.

3 Numerical identification

3.1 Optimization procedure

We have written the software package ICSE (Identification of Control of Systems in Evolution) (3) in the framework of a software system called Basile[1] (11) to solve general problems of optimization (possibly with boundary constraints) of the following form :
Let x be any state function defined on the time interval $[t_0, t_0 + t_1]$ whose values are vectors of $\mathbb{R}^{n_x}$ such that

$$\begin{cases} \dfrac{dx}{dt} = f(t,x,u) & (34) \\ x(t_0) = X_0 & (35) \end{cases}$$

where
t denotes the time variable,
X_0, vector of initial values of the state variables, is given in $\mathbb{R}^{n_x}$,

[1] All rights reserved. Basile is registered at Agence pour la Protection des Programmes, 119 rue de Flandre 75019 Paris France, serial number 87-43-003-00. Basile is an interactive interpreted software package developped at INRIA by F. Delebecque, S. Steer et al. Basile is based on the MATLAB syntax, extended with a number of powerful features, in particular a more developped data basis including polynomials, matrix polynomials, lists. The ability to support and manipulate a list data structure is the most essential difference between Basile and MATLAB : the list structure allows a natural symbolic representation of complicated mathematical objects such as transfer functions and linear systems.

f is any smooth function,
$u \in \mathbb{R}^{n_u}$ denotes the vector of parameters to be identified and that may be subject to boundary constraints of the following form

$$\text{for all } i \in \{1, \ldots, n_u\} \quad a_i \leq u_i \leq b_i \tag{37}$$

where $a_1, \ldots, a_{n_u}, b_1, \ldots, b_{n_u}$ are given in $\mathbb{R}$.
Then a value of u minimizing $J(x, u)$ is sought for, where J is a criterion estimating the difference between the model output and the measurements.

ICSE mainly consists of FORTRAN 77 routines that solve the state-system (Eq. 34-35) by the Crank-Nicholson method (9) and then compute J, the adjoint state and the gradient ∇J of J with respect to the parameters u (4). Notice that any ICSE's user has to write the routines that give $f, \frac{\partial f}{\partial x}, \frac{\partial f}{\partial u}$ and $J, \frac{\partial J}{\partial x}, \frac{\partial J}{\partial u}$.

Then, as ∇J is known, various numerical methods of optimization previously implemented in Basile (11) may be used.
In our particular case, we have chosen a quasi-Newton method with projection, where the Hessian of J is obtained by a modified BFGS method (16). It is well-known (12) that Newtonian methods provide minimum that may be local and might depend on the way that the initialization is performed.

3.2 Constants and parameters

Carrying out in our particular case, we have
$t_0 = 0$, $t_1 = 1800$ (Eq. 1)
for $M_1, M_2 : x = (x_0 \quad x_1 \quad x_2 \quad x_3)^T, n_x = 4$ and (Eq. 34) is (Eq. 7-10),
for $M_3 : x = (x_0 \quad x_1 \quad x_2 \quad x_3 \quad e)^T, n_x = 5$ and (Eq. 34) is (Eq. 7-11)
X_0 is given by Equation 3
Denoting

$$U = (u_{10}, u_{20}, u_{21}, u_{32}, u_{01}, u_{02}, u_{03}, v_{10}^m, K_{10}^m, v_{20}^m, K_{20}^m), \tag{38}$$

we have
in the simplified case $u = U$ and $n_u = 11$
in the general case $u = (U, \alpha_1, \alpha_2, \alpha_3)$ and $n_u = 14$.
Since we know that any parameter in u is nonnegative, we have chosen in Equation 36 every a_i equal to 10^{-17} and every b_i equal to 10^{17} (we verified *a posteriori* that this upper bound 10^{17} is never active) except for $\alpha_1, \alpha_2, \alpha_3$ whose upper bounds b_i have to be equal to 1 (Eq. 6).

3.3 Criterion

We have chosen an output least-square error criterion

$$J = \frac{1}{2} \sum_{i=1}^{8} \sum_{j=1}^{n_t} \sum_{k=1}^{n_y} w_{jk} \left[(y(t_j, u) - \hat{y}_{ij})(k) \right]^2 \tag{39}$$

where we denote
by n_t the number of observation times ($n_t = 11$ for M_1, M_2 and $n_t = 9$ for M_3 (Eq. 1)),

by n_y the number of measurements performed at each observation time for one of the 8 volunteers ($n_y = 2$ for M_1, M_2 and $n_y = 4$ for M_3 (Eq. 2)),
by $y(t_j, u) \in I\!R^{n_y}$ the model output (with parameters u) corresponding to one observation (Eq. 2) at the j^{th} observation time t_j ($1 \leq j \leq n_t$),
by $\hat{y}_{ij} \in I\!R^{n_y}$ the observation (Eq. 2) for the i^{th} volunteer ($1 \leq i \leq 8$) at the j^{th} observation time t_j ($1 \leq j \leq n_t$). Notice that since each amount was determined in quadruplicate, each component of $\hat{y}_{ij}$ is the mean value for 4 separate determinations
by $Y(k)$ the k^{th} component of any vector Y of $I\!R^{n_y}$ ($1 \leq k \leq n_y$)

3.4 Weights

M_1 set of experiments
We found that the previously described optimization procedure with the following classical weights leads to a final model whose ouptut is a poor approximation to the observations M_1 when considering the second components (19).
Weights **1**

$$w_{jk} = \frac{1}{[\max(\sigma_{jk}, 5 \cdot 10^{-3})]^2}$$

where σ_{jk} is the estimated standard deviation for the 4×8 results of the k^{th} measurement ($1 \leq k \leq n_y$) at the j^{th} observation time ($1 \leq j \leq n_t$).
Notice that we had to set a positive infimum for the denominator, since at the last 4 (respectively 3) observation times for M_1 (respectively M_2) no radioactivity can be detected in the platelets after degranulation (this corresponds to the second measurement) for any of the 8 volunteers. Then we have chosen $\frac{\varepsilon}{2} = 5 \cdot 10^{-3}$ as lower bound for σ_{jk}, where $\varepsilon = 10^{-2}$ is the level under which the radioactivity (expressed in 10^{-19} mol/platelet) is no longer measured.
Weights **2**

$$w_{jk} = \frac{\max\left\{\sum_{i=1}^{8} \hat{y}_{i\ell}(1); 1 \leq \ell \leq n_t\right\}}{\max\left\{\sum_{i=1}^{8} \hat{y}_{i,\ell}(k); 1 \leq \ell \leq n_t\right\}}$$

where $\hat{y}_{i\ell}(k)$ denotes the k^{th} component of $\hat{y}_{i\ell} \in I\!R^{n_y} (1 \leq k \leq n_y)$.
Notice that w_{jk} is the same for all $j \in \{1, \ldots, n_t\}$.
We intended here to equalize the orders of magnitude of the various components of the observation over the whole time-scale by equalizing the maxima of these components.
Weights **3**
Next we tried various sets of weights, and from these numerical experiments we have chosen for M_1 the weights indicated in Table 1A.

M_2 and M_3 sets of experiments
When performing numerical identification for M_2 and M_3, we observed (as for M_1) that the outputs of final models obtained at the end of optimization process with the weights **2** clearly better fit the observations than the outputs of final models found with the weights **1**. Moreover we did not succeed in finding a set of weights that conclusively improves the approximation to the observations of M_2 or M_3 obtained with the weights **2**. So we have used for M_2 and M_3 the weights **2** shown in Table 1B and 1C.

Table 1: Weights of the output least-square error criterion J for each set of experiments : $M_1(A)$, $M_2(B)$ and $M_3(C)$

	index j	1	2	3	4	5	6	7	8	9	10	11
	time $t_j(s)$	10	20	30	40	60	180	300	600	900	1200	1800
A	w_{j1}	0.1	0.1	0.1	2	5	0.1	100	100	100	100	100
	w_{j2}	0.1	0.1	2	2	5	100	100	100	100	100	100

	index j	1	2	3	4	5	6	7	8	9	10	11
	time $t_j(s)$	10	20	30	40	60	180	300	600	900	1200	1800
B	w_{j1}	1	1	1	1	1	1	1	1	1	1	1
	w_{j2}	42	42	42	42	42	42	42	42	42	42	42

	index j	1	2	3	4	5	6	7	8	9
	time $t_j(s)$	10	20	30	40	60	120	300	600	1800
	w_{j1}	1	1	1	1	1	1	1	1	1
C	w_{j2}	1	1	1	1	1	1	1	1	1
	w_{j3}	4	4	4	4	4	4	4	4	4
	w_{j4}	80	80	80	80	80	80	80	80	80

J is defined in Equation 38. For $k \in \{1,2,3,4\}$, w_{jk} weights the square of the k^{th} component of the difference between the model output and any of the observations at time t_j.

3.5 Accuracy

We have previously pointed out (cf. Section 1.3) that numerical identifiability concerns the accuracy of the parameter estimates ; its evaluation is based in our case on the square approximate covariance matrix V of parameter estimates $\bar{u}$ obtained when linearizing around $\bar{u}$ the function that relates u to $y(t,u)$, which is the output at time t of the model with parameters u. Then, keeping on denoting
by n_u the number of parameters to be identified,
by n_t the number of observation times,
by n_y the number of measurements performed at each observation time for one of the 8 volunteers,
by σ_{jk} the estimated standard deviation for the 4×8 results of the k^{th} measurement ($1 \leq k \leq n_y$) at the j^{th} observation time t_j ($1 \leq j \leq n_t$)
by w_{jk} the weight (in the criterion J (Eq. 38)) of the square of the k^{th} component ($1 \leq k \leq n_y$) of the difference between the model output and any of the 8 observations at time t_j ($1 \leq j \leq n_t$).
and denoting

$$s_{jk} = \max(\sigma_{jk}, 5.10^{-3})^2$$

we have (27)

$$V = (L^T W L)^{-1} L^T W R W L (L^T W L)^{-1}$$

where :

$$L = \begin{pmatrix} \frac{\partial y}{\partial u}(t_1, \bar{u}) \\ \frac{\partial y}{\partial u}(t_2, \bar{u}) \\ \vdots \\ \frac{\partial y}{\partial u}(t_{n_t}, \bar{u}) \end{pmatrix}, W = \begin{pmatrix} w_{11} & 0 & \cdots & \cdots & \cdots & \cdots & 0 \\ 0 & \ddots & & & & & \\ & & w_{1n_y} & & & & \\ \vdots & & & \ddots & & & \vdots \\ & & & & w_{n_t 1} & & \\ & & & & & \ddots & 0 \\ 0 & \cdots & \cdots & \cdots & \cdots & 0 & w_{n_t n_y} \end{pmatrix}$$

$$R = \frac{1}{4 \times 8} \begin{pmatrix} s_{11} & 0 & \cdots & \cdots & \cdots & \cdots & 0 \\ 0 & \ddots & & & & & \\ & & s_{1n_y} & & & & \\ \vdots & & & \ddots & & & \vdots \\ & & & & s_{n_t 1} & & \\ & & & & & \ddots & 0 \\ 0 & \cdots & \cdots & \cdots & \cdots & 0 & s_{n_t n_y} \end{pmatrix}$$

Then the square root of the i^{th} diagonal entry V_{ii} $(1 \leq i \leq n_u)$ of V is the standard deviation estimate of the i^{th} parameter u_i

3.6 Termination

When carrying out optimization, we have chosen to rescale the vector of parameters every 30 iterations (i.e. simulation calls, that is ICSE's calls to compute J and ∇J) .
Moreover, we have decided to stop (i.e. to consider the obtained parameters as optimal ones) when at least 6×30 iterations were performed and when the relative variation of the criterion J during the last 30 iterations was smaller than 10^{-4}.

3.7 Initialization

It is well-known (12) that initialization is very important when performing an iterative process of nonlinear optimization.

• **First method** :
In the beginning (first two steps) we considered the simplified case and finally (third step) we computed optimal values for all the parameters present in Equations 7-11.
Step 1.1
We set $\alpha_1 = \alpha_2 = \alpha_3 = 0$ (simplified case), and $v_{10}^m = v_{20}^m = 0$, (the Michaelis terms vanish in Equations 7-11 and thus the whole kinetic is linear).
Then we performed numerical identification of the parameters still appearing in Equations 7-11 that were

$$U_\ell = (u_{10}, u_{20}, u_{21}, u_{32}, u_{01}, u_{02}, u_{03}) \tag{40}$$

To do so, we carried out the previously described optimization procedure with the following initialization :

Let $m_1 = (\overline{x_1 + x_2 + x_3})(10), m_2 = (\overline{x_1 + x_3})(10)$ be the mean values of intra-platelet observations after the shortest observation time (i.e. 10 s) shown in Table 2.

Table 2: Mean values of intra-platelet observations at the shortest observation time (10s) for each set of experiments : M_1, M_2 and M_3

	M_1	M_2	M_3
m_1	0.220	0.250	0.250
m_2	0.060	0.040	0.052

m_1 and m_2 are the mean values of the amount (10^{-19} mol/platelet) of total and non-releasable tritiated material present in the platelet.

As a first approximation, taking into account the shortness of the incubation time (10 s) and the slowness of pool II exchanges, we considered that
$x_3(10) \approx x_3(0^+) = 0$ (Eq. 3), and so $x_1(10) \approx m_2$, $x_2(10) \approx m_1 - m_2$
Then, linearizing Equations 8-9 on the time interval $[0, 10]$ and using Equation 3 we set

$$\begin{cases} u_{10} &= m_2/10x_0(0^+) \\ u_{20} &= (m_1 - m_2)/10x_0(0^+) \end{cases} \tag{41}$$

Moreover, since it was observed that x_1 decreases quickly after 60 s and since pool I was supposed to be a way of entering into the dense granules, we chose initially $u_{10} \ll u_{21}$ and $u_{01} \ll u_{21}$ by setting

$$u_{21} = 10\ u_{10}, \quad u_{01} = u_{10} \tag{42}$$

Finally, since it was observed that x_2 increases and that $x_2 \gg (x_1 + x_3)$, and since the pool II exchanges are supposed to be slow, we chose initially $u_{32} \ll u_{21}, u_{03} \ll u_{21}$ and $u_{02} \ll u_{32}$ by setting

$$u_{32} = 10^{-3}\ u_{21}, \quad u_{03} = u_{32}, \quad u_{02} = 10^{-1}\ u_{32} \tag{43}$$

So from Equations 3 and 40-42, we obtained the initial value of U_ℓ (Eq. 17) shown in Table 3.

Table 3: Initial values of the linear kinetic constants in the simplified case for each set of experiments : M_1, M_2 and M_3

	u_{10}	u_{20}	u_{21}	u_{32}	u_{01}	u_{02}	u_{03}
M_1	$1.5\ 10^{-4}$	4.10^{-4}	$1.5\ 10^{-3}$	$1.5\ 10^{-6}$	$1.5\ 10^{-4}$	$1.5\ 10^{-7}$	$1.5\ 10^{-6}$
M_2	2.10^{-5}	10^{-4}	2.10^{-4}	2.10^{-7}	2.10^{-5}	2.10^{-8}	2.10^{-7}
M_3	$1.5\ 10^{-4}$	5.10^{-4}	$1.5\ 10^{-3}$	$1.5\ 10^{-6}$	$1.5\ 10^{-4}$	$1.5\ 10^{-7}$	$1.5\ 10^{-6}$

Elements of U_ℓ (cf. Equation 39), biologically defined in Section 1.2 of the text, and expressed in s^{-1}.

The experimental results suggest that the dynamics have both fast and slow mode. So we used two time scales (times are expressed in s) : on the time interval $[0, 120]$ (respectively [120,1800]) we chose the step 0.5 (respectively 1) These steps were chosen after solving exactly the state-system (Eq. 7-10) for M_1 in this simplified linear case with the initial constants for

M_1 shown in Table 3 and then computing the errors in the model outputs: we wanted no error to be greater than 10^{-6}.

Step 1.2

We performed numerical identification of the parameters appearing in Equations 7-11 in the simplified case, that were the elements of U (Eq. 37).

To do so, we carried out the previously described optimization procedure with the following initialization :

We set as initial values of the elements of U_ℓ (Eq. 39) the values obtained at the end of Step 1.1, except for u_{10} and u_{20}. We divided the uptake kinetic at time 0 found at the end of Step 1.1 equally in a linear part and in a Michaelis part. So for $i = 1, 2$ we set half of the value of u_{i0} found at the end of the Step 1.1 as initial value of u_{i0} and of $\dfrac{v_{i0}^m}{K_{i0}^m + x_0(0^+)}$.

According to Anderson et al. (1), the Michaelis constant k_m for platelet uptake is approximately 0.5 μM. As our experimental results are expressed in 10^{-19} mol/platelet, we got from the experimental protocol described in Section 1.1 the following initial value K_m of K_{10}^m and K_{20}^m :

for M_1 and M_3, $K_m = 100 \times 10^{-19}$ mol/platelet, and for M_2, $K_m = 550 \times 10^{-19}$ mol/platelet.

As in Step 1.1, we used two time scales (times are expressed in s) : on the time interval $[0, 120]$ (respectively [120,1800]) we chose the step dti (respectively dtf). During the first 9×30 iterations (i.e. simulation calls), we chose dti = 0.5 and dtf = 1 : during the last iterations, to get a better accuracy, we chose dti = 0.1 and dtf = 0.5. These last steps were chosen after solving exactly the state-system (Eq. 7-10) for M_1 in the simplified linear case with the parameters obtained at the end of the optimization procedure, and then computing the errors in the model outputs: we wanted no error to be greater than 10^{-6}.

Step 1.3

We considered the general case, and we performed numerical identification of the parameters appearing in Equations 7-11 that were the elements of $(U, \alpha_1, \alpha_2, \alpha_3)$, U being defined in Equation 37.

To do so, we carried out the previously described optimization procedure with the following initialization :

We set as initial value of U (Eq. 37) the value obtained at the end of Step 1.2.

We set 10^{-5} as initial value of α_1, α_2 and α_3.

We used the same time scales as in Step 1.1.

• **Second method** :

We did not consider the simplified case, but simply performed in the general case optimization procedures analogous to those of Steps 1.1 and 1.2.

Step 2.1

We considered that the whole kinetic was linear, and we performed numerical identification of the parameters still appearing in Equations 7-11 that were the elements of $(U_\ell, \alpha_1, \alpha_2, \alpha_3)$, U_ℓ being defined in Equation 39.

To do so, we carried out the previously described optimization procedure with the initial value of U_ℓ (Eq. 39) shown in Table 3 and with (0.5, 0.1, 0.1) as initial value of $(\alpha_1, \alpha_2, \alpha_3)$.

We used the same time scales as in Step 1.1.

Step 2.2

We performed numerical identification of the parameters appearing in Equations 7-11 that were the elements of $(U, \alpha_1, \alpha_2, \alpha_3)$, U being defined in Equation 37.

To do so, we carried out the previously described optimization procedure with the following initialization :

We set as initial values of the elements of U_ℓ (Eq. 39) and of $(\alpha_1, \alpha_2, \alpha_3)$ the values obtained at the end of Step 2.1, except for u_{10} and u_{20}. For $i = 1, 2$ we set half of the value of u_{i0} found at the end of Step 2.1 as initial value of u_{i0} and of $\frac{v_{i0}^m}{K_{i0}^m + x_0(0^+)}$.

We chose $K_m = 100$ (respectively 550) as initial value of K_{i0}^m, $1 \leq i \leq 2$ for M_1, M_3 (respectively for M_2).

We used the same time scales as in Step 1.2.

4 Results and discussion

4.1 Results

Computations were performed on a SUN 3/60 computer with 12 megabytes of main memory.

• When carrying out optimization procedure described in section 2.2, it turned out that :

for the groups of experiments M_1 and M_2, the criterion obtained at the end of Step 1.3 is smaller than the criterion obtained at the end of Step 2.2

for the set of experiments M_3, the criterion obtained at the end of Step 2.2 is smaller than the criterion obtained at the end of Step 1.3.

The optimal values of the parameters present in Equations 7-11 shown in Table 4 were obtained when initializing with the first method (respectively the second method) for M_1, M_2 (respectively M_3).

• Figure 2 (respectively 3) shows the observations M_1 (respectively M_2) compared to homologous outputs of the initial linear simplified (A,B) and final optimal general (C,D) model corresponding to M_1 (respectively M_2).

• Figure 4 shows the observations M_3 compared to homologous outputs of the initial linear general (A,B,E,F) and final optimal general (C,D,G,H) model corresponding to M_3.

It appears in Fig. 2A,B, Fig. 3A,B and Fig. 4A,B,E,F that the initial models (curves) whose parameters where based on early observations (cf. Section 3.7 Step 1.1) are well-suited for only the first tens of seconds, and present an obvious lack of fit for longer periods of times. The power of the reported numerical identification technique appears when considering Fig. 2C,D, Fig. 3C and Fig. 4C,G,H which show optimized model curves that fit the whole observed phenomenon.

Notice that Fig. 3D shows optimized-model outputs (curve) which are of the same order of magnitude as the experimental data ; however the spike of the model curve is less sharp and high than the observed one.

As noted previously (Sections 1.1 and 1.2) the initial amount of extra-platelet [^{3}H]5-HT for M_2 was 220×10^{-19} mol/platelet, while keeping the saturating initial concentration of 2×10^{-7} M. We thus intended to delay the depletion of 5-HT in the external medium and investigate the correlation between non-releasable [^{3}H]material taken up and extra-platelet [^{3}H]5-HT. We observe (inset) the same evolution of the amount of non-releasable intra-platelet [^{3}H]material (zero after a sharp spike) for M_1 and M_2.

Finally Fig. 4D shows an optimized-model curve which presents no spike and so is a poor approximation to the observed phenomenon.

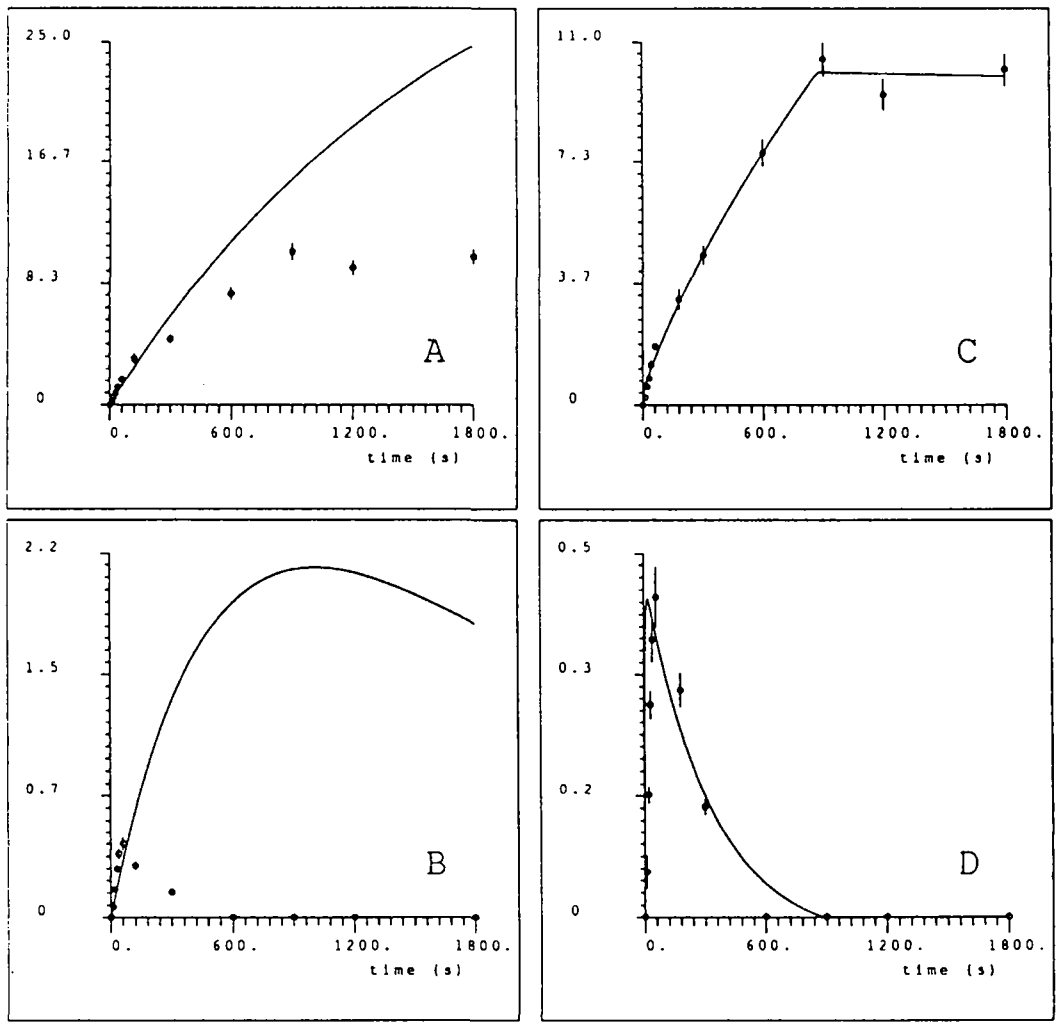

Figure 2: M_1 set of experiments (means ± SD of 4 × 8 determinations) compared to initial (A,B) and optimized (C,D) model outputs (curves). The amounts of intra-platelet [^{3}H]material are shown in A and C. The amounts of intra-platelet non-thrombin-releasable [^{3}H]material are shown in B and D (see section 1.1 Experimental protocol). Amounts are expressed in 10^{-19} mol/platelet.

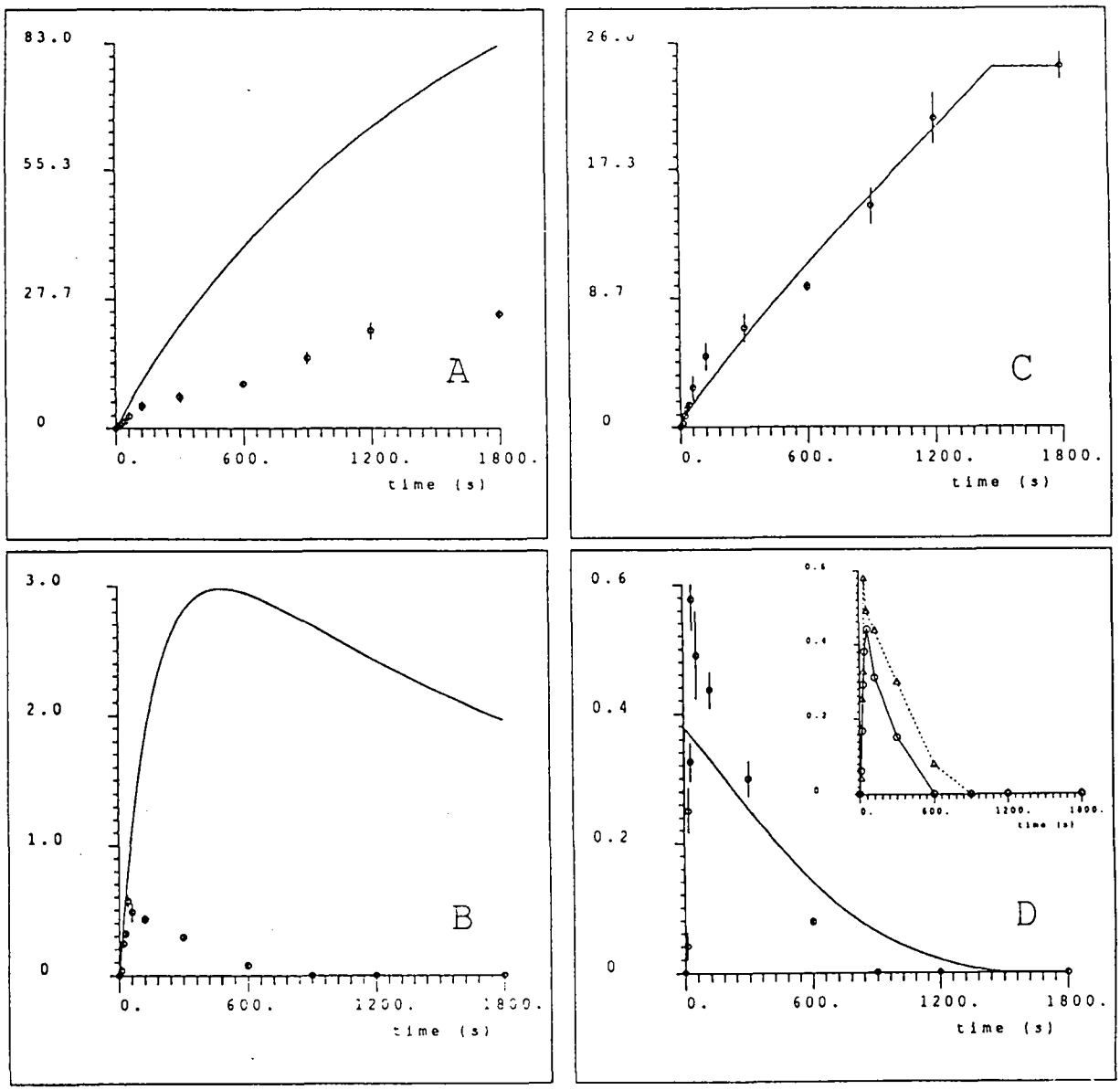

Figure 3: M_2 set of experiments (means ± SD of 4 × 8 determinations) compared to initial (A,B) and optimized (C,D) model outputs (curves). The amounts of intra-platelet [^{3}H]material are shown in A and C. The amounts of intra-platelet non-thrombin-releasable [^{3}H]material are shown in B and D (see section 1.1 Experimental protocol). Amounts are expressed in 10^{-19} mol/platelet. The insert shows the experimental kinetics of non-releasable [^{3}H]material taken up after incubation with an initial amount of [^{3}H]5-HT binoxalate per platelet increased 5.5-fold (Δ) as compared with the more commonly-used initial amount (○) (means ± SD of 4 × 8 determinations). Amounts are expressed in 10^{-19} mol/platelet.

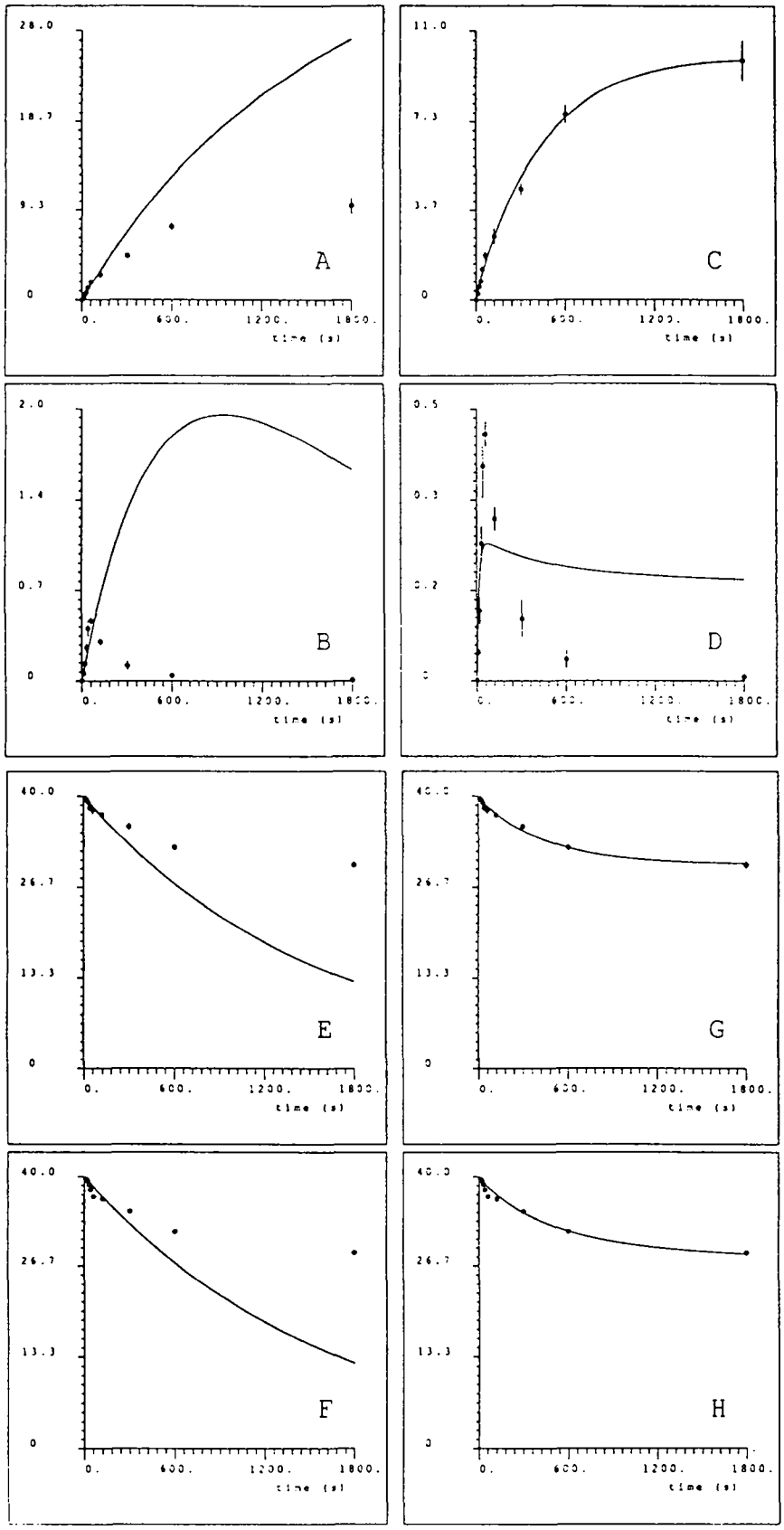

Figure 4: M_3 set of experiments (means ± SD of 4×8 determinations) compared to initial (A,B,E,F) and optimized (C,D,G,H) model outputs (curves). The amounts of intra-platelet [^{3}H]material are shown in A and C. The amounts of intra-platelet [^{3}H]material are shown in B and D. The amounts of extra-platelet [^{3}H]material are shown in E and G. The amounts of extra-platelet [^{3}H]5-HT (as measured by radiochromatography) are shown in F and H (see section 1.1 experimental protocol).Amounts are expressed in 10^{-19} mol/platelet.

• Figure 5 shows the observations M_3 compared to homologous outputs of the final optimal general model corresponding to M_1 (curves in Fig. 5A and B are those already shown in Fig 2C and D).

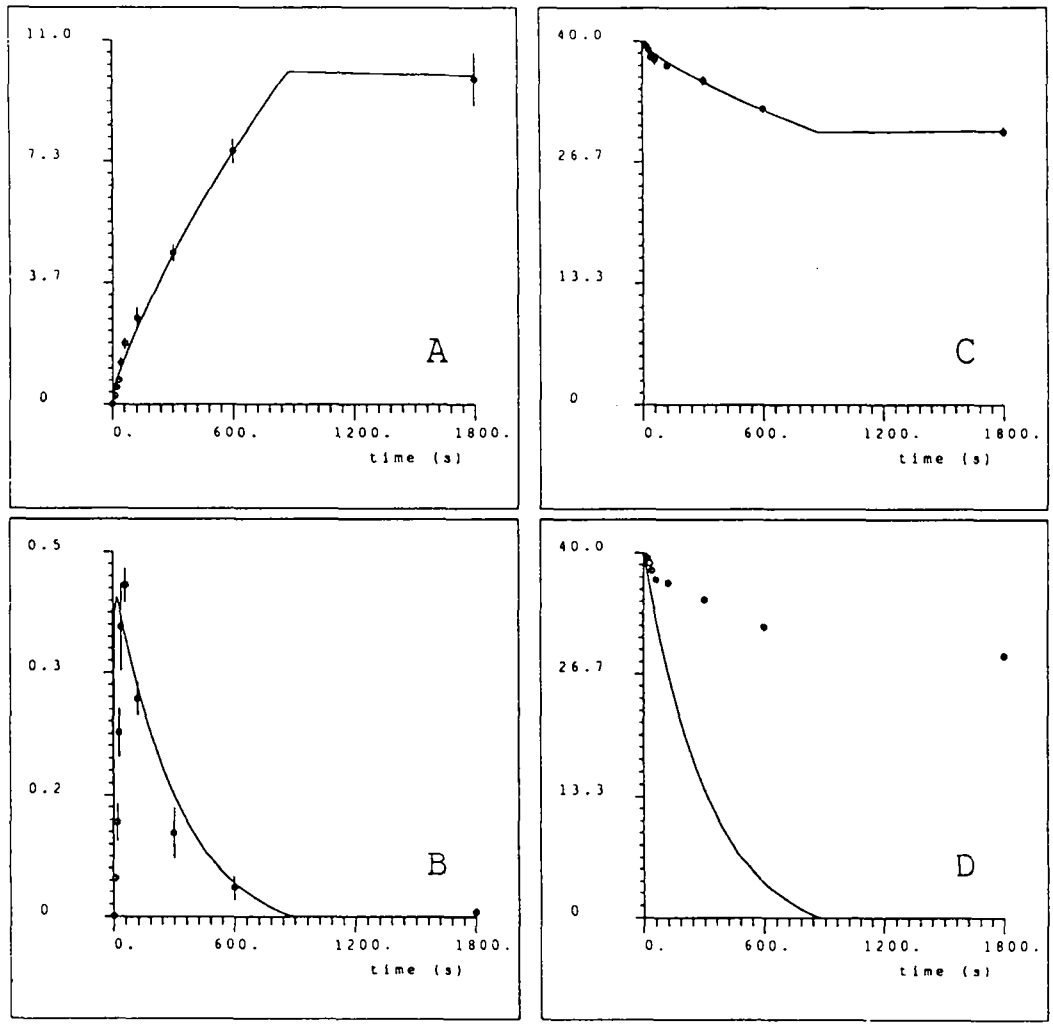

Figure 5: Optimized-model outputs (curves) obtained from M_1 set of experiments (the curves in Fig. 5A,B are those already shown in Fig. 2C,D) compared to the experimental data (already shown in Fig. 4) of M_3 set of experiments (means $\pm$ SD of 4×8 determinations). The amounts of intra-platelet [^{3}H]material are shown inFig. 5A (the experimental data are those already shown in Fig. 4A,C). The amounts of intra-platelet non-thrombin-releasable [^{3}H]material are shown in Fig. 5B (the experimental data are those already shown in Fig. 4B,D). The amounts of extra-platelet [^{3}H]material are shown in Fig. 5C (the experimental data are those already shown in Fig. 4E,G). The amounts of extra-platelet [^{3}H]5-HT are shown in Fig. 5D (the experimental data are those already shown in Fig. 4F,H).

It appears that the optimal model (curves) computed to suit M_1 fits the first three components of M_3 (Fig. 5A : total uptake, Fig. 5B : intra-platelet non-thrombin-releaseable material, Fig. 5C : extra-platelet [^{3}H]material), but gives a poor approximation to the fourth component of M_3 (Fig. 5D : extra-platelet [^{3}H]5-HT). Indeed Fig. 5D shows that the model curve fits the experimental data only until 40 s, and after this time is far below.

4.2 Discussion

The data presented here re-assert the existence of both releasable (dense granules) and non-releasable pools for 5-HT in normal platelets. This model was reported initially by Costa et al. ((6), (8)), but has not been examined subsequently.

Table 4: Optimal values of the kinetic constants for each set of experiments M_1, M_2 and M_3

	u_{10}	u_{20}	u_{21}	u_{32}	u_{01}	u_{02}	u_{03}
M_1	$2.77\ 10^{-3}$ $\pm 2.45\ 10^{-4}$	$2.18\ 10^{-4}$ $\pm 1.42\ 10^{-4}$	10^{-15}* $\pm 1.5\ 10^{-2}$	10^{-15}* $\pm 2.99\ 10^{-8}$	$2.47\ 10^{-1}$ $\pm 1.77\ 10^{-2}$	$1.25\ 10^{-5}$ $\pm 1.20\ 10^{-6}$	$1.6\ 10^{-6}$* $\pm 1.21\ 10^{6}$
M_2	10^{-17}* $\pm 5.74\ 10^{-5}$	$2.55\ 10^{-5}$* $\pm 1.20\ 10^{-4}$	$2.55\ 10^{-17}$* $\pm 2.94\ 10^{-2}$	$2.55\ 10^{-17}$* $\pm 1.90\ 10^{-6}$	1 $\pm 7.37\ 10^{-2}$	10^{-15}* $\pm 2.44\ 10^{-4}$	$2.11\ 10^{-7}$* $\pm 8.05\ 10^{6}$
M_3	$4.53\ 10^{-4}$ $\pm 1.57\ 10^{-5}$	$5.49\ 10^{-4}$* $\pm 1.21\ 10^{-3}$	10^{-17}* $\pm 7.96\ 10^{-4}$	10^{-17}* $\pm 7.59\ 10^{-7}$	$6.91\ 10^{-2}$ $\pm 7.89\ 10^{-4}$	$1.6\ 10^{-3}$ $\pm 1.23\ 10^{-4}$	$3.10\ 10^{-3}$* $\pm 9.03\ 10^{9}$

	v_{10}^m	K_{10}^m	v_{20}^m	K_{20}^m	α_1	α_2	α_3
M_1	$1.56\ 10^{-2}$ $\pm 5.62\ 10^{-3}$	$1.33\ 10^{2}$ ± 1.38	$9.04\ 10^{-3}$ $\pm 9.23\ 10^{-4}$	$2.14\ 10^{-2}$* $\pm 8.23\ 10^{-1}$	10^{-5}* $\pm 4.28\ 10^{-3}$	10^{-5}* $\pm 1.75\ 10^{-4}$	10^{-5}* ± 4
M_2	$9.18\ 10^{-1}$ $\pm 5.66\ 10^{-2}$	$3.14\ 10^{2}$ $\pm 1.08\ 10^{2}$	$1.40\ 10^{-2}$* $\pm 1.07\ 10^{-1}$	$4.6\ 10^{-3}$* $\pm 5.69\ 10^{5}$	10^{-5}* ± 4.29	10^{-5}* $\pm 2.95\ 10^{-3}$	10^{-5}* $\pm 4.51\ 10^{5}$
M_3	10^{-17}* $\pm 6.58\ 10^{-4}$	$4.47\ 10^{2}$* $\pm 7.50\ 10^{9}$	10^{-17}* $\pm 3.95\ 10^{-1}$	$2.87\ 10^{2}$* $\pm 2.21\ 10^{10}$	$9.31\ 10^{-1}$ $\pm 8.01\ 10^{-4}$	10^{-1} $\pm 1.22\ 10^{-4}$	10^{-1}* $\pm 2.74\ 10^{10}$

Parameters present in Equations 7-11 (optimal values $\pm$ SD). * numerically unidentifiable parameter

• From Table 4 it appears that :

for the first two sets of experiments, M_1, M_2, the parameters $\alpha_1, \alpha_2, \alpha_3$ are unidentifiable. Indeed, M_1 and M_2 provide only intra-platelet observations that one could expect to be much less sensitive to the $(\alpha_i)_{1\leq i\leq 3}$ than measurements in the external medium.

for any set of experiments, M_1, M_2 and M_3, the parameters $u_{21}, u_{32}, u_{03}, K_{20}^m, \alpha_3$ are unidentifiable.

Notice that from the kinetics of the amount of intra-platelet non-releasable [^{3}H]material (zero after a sharp spike), we could expect numerical unidentifiability of u_{32}, u_{03} and α_3 that are kinetic constants related with pool II, since this pool II seems to be unaffected by the uptake of 5-HT at the measurement times.

In contrast, the unidentifiability of u_{21} and K_{20}^m was unexpected. Notice that the outputs of the optimized model corresponding to M_1 are poorly sensitive to u_{21} ; indeed they are not significantly different (Student's test) for $u_{21} \in [10^{-15}, 10^{-3}]$. Under these conditions the flux of exchanged [^{3}H]material from pool I to dense granules ($u_{21}x_1$) remains small with respect to other fluxes related to the external medium (i.e. for maximal values 4.10^{-4} as compared with 3.10^{-3} to $10^{-1} \times 10^{-19}$ mol/platelet $\times$ s).

The unidentifiability of K_{20}^m remains to be explained. Indeed, our evaluation of the accuracy of the parameter estimates is based on an approximate covariance matrix obtained by linearization. Such an approximation, although very common, is questionable (31).

Moreover these unidentifiability problems are probably not only due to noisy data, but may well be numerical problems resulting from large differences in magnitude. Consider qualitatively the expression $u + \dfrac{v_m}{K_m + x_0}$. All three parameters can be shown to be structurally identifiable, but depending on the relative magnitude of the parameter K_m and the state variable x_0, it is foreseeable that numerical difficulties may arise, e.g. (i) $K_m \gg x_0$: probably the three parameters are numerically identified as a group (ii) $K_m \ll x_0$: numerical identification of K_m might be difficult.

• As is well-known (10), the vesicular-releasable-pool appears to be the platelet dense-granule storage 5-HT compartment : 5-HT enters this compartment more rapidly than it leaves (Table 4).
However, from the experimental data, only one non-releasable pool appears instead of the pools I and II (8) which have never been ultrastructurally defined. This apparent discrepancy might be due to differences between experimental protocols :

only one [^{3}H]5-HT concentration (2×10^{-7} M) was used instead of 10^{-8} to 10^{-5} M (8),
the duration of uptake experiments was 10 s to 30 min (Eq. 1) instead of 10 s to 4 h (8),
and 5-HT binoxalate was used instead of 5-HT creatinine sulphate complex (8).

It may well be that pool II simply represents 5-HT which has been lost from the dense granules into the cytoplasm, from which it will slowly exit from the cell. As a consequence, it may be seen only under conditions which predispose to loss of 5-HT from the dense granules, such as flooding the system with 5-HT (high initial 5-HT concentrations) or leakage during prolonged incubation. It may well represent some type of metabolite (deaminated or sulfated). Moreover, the molecular conformation of 5-HT might be as important for the carrier system as for the receptors (14).
It should also be noted that storage pool deficient platelets of cattle (devoid of dense granules) exhibit only one 5-HT compartment, as evidenced by ^{19}F-N M R of 4,6-difluoro-5-HT (21).

One interpretation would be the inclusion of pool II into dense granules, as reported for chromaffin granules (24). This is not supported by the present modeling, since the non-releasable outputs ($x_1 + x_3$) of the optimized model corresponding to M_1 are poorly sensitive to variations of both K_{20}^m and v_{20}^m: indeed they are not significantly different except for one of their 11 components (Student's test) for $v_{20}^m \in [6.5 10^{-3}, 3.10^{-2}]$ and $K_{20}^m \in [0,2]$

Another interpretation would be metabolism : the fluorinated analog of 5-HT used in cattle platelets has been considered to be sequestered in the non-releasable pool II (21), which may represent metabolized 5-HT. 4,6-difluoro-5-HT appears to be an excellent substrate for M-phenolsulphotransferase (EC 2.8.2.1.), an enzyme partly associated with the dense-body membrane like other 5-HT metabolizing enzymes (18).

• Under the present experimental conditions, only the releasable compartment and the non-releasable pool I were explored : and the existence of pool I, difficult to assess experimentally, was demonstrated. The non-releasable pool might be related to the existence of platelet-derived molecules (actin (26), serotonin binding proteins (20)) able to bind 5-HT, or to sequestration in α-granules or lysosome-like structures not released by brief thrombin treatment.

According to our model, dense bodies accumulate 5-HT mainly from the extracellular medium rather than via uptake into an intra-platelet non-releasable 5-HT compartment, and both compartments have direct access to extracellular 5-HT. This is consistent with a previous hypothesis (8). Interestingly, an anchorage of dense granules on the platelet plasma membrane has recently been shown in the absence of any secretory stimulation (22). Consequently extracellular 5-HT could cross both the cytoplasmic and the vesicular membranes by means of "specific channels". Thus 5-HT could reach the interior of the vesicles without being truly "free" in the intra-platelet matrix.

• Finally, it should be emphasized that the optimized model corresponding to M_1 fits total uptake, non-releasable and extracellular [^{3}H]material kinetics for M_3 (Fig. 5A,B,C). In this context, a poor approximation to extracellular [^{3}H]5-HT kinetics was obtained (Fig. 5D) :

indeed, as predicted by the model curve, the amounts of 5-HT were much lower than those measured experimentally. This challenges the radiochromatographic measurements of "apparently authentic" 5-HT which however could include oxidation products derived from the extracellular 5-HT. Note that 15 oxidative products of 5-HT, some of which comigrate with 5-HT, have been recently identified (32).

Acknowledgements: The authors are indebted to Martine Verneuille for secretarial assistance and to Bernard Boursin for photographical aid.

References

(1) ANDERSON G.M., J.M. STEVENSON, AND D.J.COHEN. Steady state model for plasma free and platelet serotonin in man. *Life Sci.* 41: 1777-1785, 1987.

(2) BERGMAN R.,, AND C. COBELLI. Minimal modeling partition analysis, and the estimation of insulin sensitivity. *Fed. Proc.* 39: 110-115, 1980.

(3) BONNANS J.F., AND G. LAUNAY. ICSE In : *Basile Version 2.0.* INRIA, Rocquencourt, 1988.

(4) CLARKE F.H. *Optimization and non smooth analysis.* J. Wiley and Sons, New York, 1983.

(5) COSTA J.L., AND D.L. MURPHY. Platelet 5-HT uptake and release stopped rapidly by formaldehyde. *Nature* 255: 407-408, 1975.

(6) COSTA J.L., S.A. SILBER, AND D.L. MURPHY. Effects of reserpine and imipramine on vesicular serotonin uptake and storage in intact human platelets. *Life Sci.* 21: 181-188, 1977.

(7) COSTA J.L., Y. TANAKA, K.D. PETTIGREW, AND R.J. CUSHING. Evaluation of the utility of air-dried whole mounts for quantitative electron microprobe studies of platelet dense bodies. *J. Histochem. Cytochem.* 25:1079-1086, 1977.

(8) COSTA J.L., K.L. KIRK, D.L. MURPHY, AND H. STARK. Anomalous compartmentation of 5-hydroxytryptamine in intact human platelets. *Brit.J. Pharmacol.* 72: 449-459, 1981.

(9) CROUZEIX M., AND A.L. MIGNOT. *Analyse numérique des équations différentielles.* Masson, Paris, 1984.

(10) DA PRADA M., J.G. RICHARDS, AND R. KELLER. Amine storage organelles in platelets. in : *Platelets in Biology and Pathology 2-* (Gordon J.L. Ed. Elsevier, Amsterdam) 105-145, 1981.

(11) DELEBECQUE F., C. KLIMANN, AND S. STEER. *Basile Version 2.0.*, INRIA, Rocquencourt, 1988.

(12) DENNIS J.E., AND R.B. SCHNABEL. *Numerical methods for unconstrained optimization and nonlinear equations.* Prentice-Hall, Inc. , Englewood Cliffs, New Jersey, 1983.

(13) DETWILLER T.C., AND R.D. FEINMANN. Kinetics of the thrombin-induced release of calcium (II) by platelets. *Biochemistry* 12: 282-289, 1973.

(14) EDVARDSEN O., AND S.G. DAHL. Molecular structure and dynamics of serotonin. *Mol. Brain Res.* 9: 31-37, 1991.

(15) FAY D.D., J.L. COSTA, AND J.M. LAUNAY. Thin-layer-chromatographic separation and quantitation of radioactivity-labelled-5-hydroxytryptamine, 5-hydroxytryptamine-O-sulfate, and 5-hydroxyindoleacetic acid. *J. Chromatogr.* 252: 338-341, 1982.

(16) FLETCHER R. *Practical methods of optimization.* J. Wiley and Sons, New York, 1987.

(17) GODFREY K.R., AND J.J. DISTEFANO III. Identifiability of model parameters In : *Identifiability of parametric models.* E. Walter (ed.), chapter 1, 1-20, Pergamon Press, 1988.

(18) JOLIVET-REYNAUD C., J.M. LAUNAY, AND J.E. ALOUF. Damaging effects of clostridium perfringens delta toxin on blood platelets and their relevance to ganglioside G_{M2}. *Arch. Biochem. Biophys.* 262: 59-66, 1988.

(19) LAUNAY G. *Modélisation du stockage de la sérotonine dans les plaquettes humaines.* Thèse de l'Université de Paris IX-Dauphine, 1989.

(20) LIU K.P., H. TAMIR, AND M. ADLERSBERG. Photoaffinity labeling of the two forms of serotonin binding protein : peptide mapping of the binding sites. *J. Neurochem.* 54: 963-970, 1990.

(21) MEYERS K.M., J.L. COSTA, AND J. MAGNUSON. Compartmentation of 4,6-difluoro-5-HT studied by nuclear magnetic resonance in normal and CHS bovine platelets. *Thromb. Res.* 58: 265-272, 1990.

(22) MORIMOTO T., S. OGIHARA, AND H. TAKISAWA. Anchorage of secretion-competent dense granules on the plasma membrane of bovine platelets in the absence of secretory stimulation. *J. Cell Biol.* 111: 79-86, 1990.

(23) MURPHY D.L., R.W. COLBURN, J.M. DAVIS, AND W.E. BUNNEY Jr. Stimulation by lithium of monoamine uptake in human platelets. *Life Sci.* 8: 1187-1193, 1969.

(24) PLETSCHER A., M. DA PRADA, K.H. BERNEIS, H. STEFFEN, B. LUTOLD, AND H.G. WEDER. Molecular organisation of amine storage organelles of blood platelets and adrenal medulla. *Adv. Cytopharmacol.* 2: 257-264, 1974.

(25) PLETSCHER A. (ed.). The platelet in Pathophysiological Research. *Experientia* 44: 91-154, 1988.

(26) SMALL D.H., AND R.J. WURTMAN. Binding of ^3H serotonin to skeletal muscle actin. *J. Neurochem.* 45: 819-824, 1985.

(27) SORENSON H.W. *Parameter Estimation, Principles and Problems.* M. Dekker, New York, 1980.

(28) STAHL S.M., AND H.Y. MELTZER. A kinetic and pharmacologic analysis of 5-hydroxytryptamine transport by human platelets and platelet storage granules : comparison with central serotoninergic neurons. *J. Pharmacol. Exp. Ther.* 205: 118-132, 1978.

(29) VAJDA S., K.R. GODFREY, AND H. RABITZ. Similarity transformation approach to identifiability analysis of nonlinear compartmental models. *Math. Biosc.* 93: 217-248, 1989.

(30) WALTER E., AND Y. LECOURTIER. Unidentifiable compartmental models : what to do ?. *Math. Biosc.* 56: 1-25, 1981.

(31) WALTER E., AND H. PIET-LAHANIER. Estimation of parameter uncertainty resulting from bounded error-data. *Math. Biosc.* 92: 54-74, 1988.

(32) WRONA M.Z., AND G. DRYHURST. Electrochemical oxidation of 5-hydroxytryptamine in aqueous solution at physiological pH. *Bioorganic Chem.* 18: 291-317, 1990.

Unité de Recherche INRIA Rocquencourt
Domaine de Voluceau - Rocquencourt - B.P. 105 - 78153 LE CHESNAY Cedex (France)

Unité de Recherche INRIA Lorraine Technopôle de Nancy-Brabois - Campus Scientifique
615, rue du Jardin Botanique - B.P. 101 - 54602 VILLERS LES NANCY Cedex (France)
Unité de Recherche INRIA Rennes IRISA, Campus Universitaire de Beaulieu 35042 RENNES Cedex (France)
Unité de Recherche INRIA Rhône-Alpes 46, avenue Félix Viallet - 38031 GRENOBLE Cedex (France)
Unité de Recherche INRIA Sophia Antipolis 2004, route des Lucioles - B.P. 93 - 06902 SOPHIA ANTIPOLIS Cedex (France)

EDITEUR
INRIA - Domaine de Voluceau - Rocquencourt - B.P. 105 - 78153 LE CHESNAY Cedex (France)

ISSN 0249 - 6399